Scientia Iranica, Vol. 14, No. 3, pp 240–250

SCIENTIA IRANICA

Large Eddy Simulation of Multiple Jets into a Cross Flow

M. Ramezanizadeh[1], M. Taeibi-Rahni[1,2] and M.H. Saidi*

Multiple square cross section jets into a cross flow at three different velocity ratios, namely 0.5, 1.0 and 1.5, have been computationally simulated, using the Large Eddy Simulation (LES) approach. The finite volume method is applied in the computational methodologies, using an unsteady SIMPLE algorithm and employing a non-uniform staggered grid. All spatial and temporal terms in the Navier-Stokes equations have been discretized using the Power-Law and Crank-Nicolson schemes, respectively. Mean velocity profiles at different X-locations are compared with the existing experimental and Reynolds Averaged Navier-Stokes (RANS) computational results. Although the RANS computations require much fewer computational resources than the LES, the authors' results show reasonably good agreement with existing experimental results, rather than the computational ones. It is shown that, by increasing the velocity ratio, the jet penetration into the cross flow is increased, accompanied by a high mixing with the cross flow. In addition, the formation of counter rotating vortex pairs after the jet enters the cross flow is explained and its behavior in different YZ-planes is investigated.

INTRODUCTION

Jet into cross flow simulation has relevance to active flow control, which is presently an area of intense interest in the research community. It has several applications, including pollutants dilution, flame stabilization, fluid mixing, the take-off or landing behavior of V/STOL airplanes and gas turbine blade surface protection from hot gas flow, namely film cooling, etc.

There are several parameters affecting the characteristics of jets into a cross flow, such as injection angle, relative spacing of the injection holes, velocity ratio, density ratio, state of the oncoming boundary layer, ratio of the boundary layer thickness to the injection hole diameter, surface curvature, longitudinal pressure gradient and free stream turbulence level, etc. Among these, the penetration of jets into the main flow depends strongly on the jets to cross flow velocity ratio, R, and/or injection angle, α. For large α's and R's, the flow is of a wake character and is similar to the flow past a solid cylinder placed on the wall. Downstream of the bending-over jet, a reverse flow zone develops, in which the hot gas is mixed in from the sides. Past the reversed-flow zone, the jet reattaches on the surface. On the other hand, at small velocity ratios, the jet bends over very quickly and attaches to the wall. Also, when the injection angle is small, the jet attaches quickly to the wall, while at higher velocity ratios, the flow develops a characterizing wall-jet.

Jet penetration and the mixing characteristics of multiple jets into a cross flow are three-dimensional phenomena and have been the object of research for many years [1-14]. Andreopoulos [1] presented spectral analysis and flow visualization for various velocity ratios and Reynolds numbers of a jet issuing perpendicularly from a developing pipe flow into a cross flow. His experimental investigations revealed the existence of large-scale structures in the jet flow. These structures were sometimes well organized, depending, basically, on the Reynolds number and the jet to cross flow velocity ratio. He also noted that, at high velocity ratios, say $R > 3$, and low Reynolds numbers, say Re < 5000, the annular mixing layer of the pipe rolls up and toroidal vortices are formed, similar to those of a jet issuing into 'still' air. These well organized vortices, or vortical rings (large structures), carry a vorticity of the same sign as the ones inside the pipe, but opposite

1. *Department of Mechanical Engineering, Sharif University of Technology, Tehran, I.R Iran.*
2. *Department of Aerospace Engineering, Sharif University of Technology, Tehran, I.R. Iran.*
*. *Corresponding Author, Department of Mechanical Engineering, Sharif University of Technology, Tehran, I.R. Iran.*

to those of the cross-stream turbulent flow. As the velocity ratio decreases, the organization of these large structures reduces, but still there exists a periodicity in their appearance. As the Reynolds number increases, say Re $>$ 5000, the regularity of the appearance of the large structures leaving the pipe decreases and the eddies now have a wide range of sizes. Finally, the average vorticity content of jets into a cross flow far downstream of the jet exit seems to be qualitatively independent of the Reynolds number for velocity ratios less than about 2.0.

Lee et al. [2] conducted an experimental study to investigate the flow characteristics of streamwise 35° inclined jets, injected into a turbulent cross flow boundary layer of a flat plate. In their work, the flow was visualized by Schlieren photographs, for both normal and inclined jets, to determine the overall flow structure with the variation of the velocity ratio. They measured the three-dimensional velocity field for two velocity ratios of 1.0 and 2.0, using a five-hole directional probe. Their visualization study showed that the variation of the injection angle causes a significant change in the flow structure. Also, they found that the jet flow is mainly dominated by turbulence for small velocity ratios, but is likely to be influenced by inviscid vorticity dynamics for large velocity ratios. Also, a pair of bound vortices accompanied by a complex three-dimensional flow is present downstream of the jet exit, as in the case of the normal injection whose range and strength depend on the velocity ratio. They concluded that the three-dimensional flow characteristics are so dominated that the previous two-dimensional measurements in the symmetry plane are not sufficient to account for the flow structure of the jets into the cross flow, especially for large velocity ratios. Their work also showed that, when the velocity ratio is small, the fluid from the jet exit is bent towards the wall. Therefore, it seems that only the injected fluid in some downstream region of the jet exit exists. However, for large velocity ratios, the injected jet is separated from the wall abruptly, such that only the cross flow fluid is filled in the region between the wall and the jet trajectory.

Ajersch et al. [3] have both experimentally and computationally studied the flow of a row of six square jets injected perpendicularly to a cross flow. Their jet to cross flow velocity ratios were 0.5, 1.0 and 1.5, while their jet spacing to jet width ratio was 3.0. Also, their jet Reynolds number was 4700. They measured the mean velocities and the six Reynolds stresses, using a three-component Laser Doppler Velocimeter (LDV) operating in coincidence mode. Their computational flow simulation was performed using a multi-grid, segmented, k ε computational fluid dynamic code. Their special near wall treatment included a non-isotropic formulation of the effective viscosity, a low Reynolds number model for k and an algebraic model of the flow length scale. Their computational domain included the jet channel, as well as the flow above it. In their work, the flow velocities and Reynolds stresses on the jet centerline, downstream of the jet exit, were not predicted very well, probably due to the inadequate turbulence model used. However, the values off the centerline matched reasonably well with those of their experiments.

Holdeman and Walker [4] developed an empirical model for predicting the temperature distribution downstream of a row of dilution jets injected normally into a heated cross flow in a constant area duct. Their model was based on the assumption that all properly non-dimensionalized vertical temperature profiles can be expressed in a self-similar form. They claimed that their results were in excellent agreement with the experimental data, except for the combinations of the flow and the geometric variables, which resulted in a strong impingement on the opposite wall.

Hoda and Acharya [5] studied the performance of seven different existing turbulence models (a high-Re model, three low-Re models, two non-linear models and a Direct Numerical Simulation (DNS) based low-Re model) for the prediction of film coolant jets injected normally into a cross flow. They compared their results of different models with the experimental data of Ajersch et al. [3] and with each other to critically evaluate the performance of those models. They claimed that close agreement with the experimental results were obtained at the jet exit and far downstream of the injection region using different models. However, all models used typically over-predicted the magnitude of the velocities in the wake region behind the jet.

Keimasi and Taeibi-Rahni [6] also computationally studied a three-dimensional turbulent flow of jets injected perpendicularly into a cross flow. They applied the Reynolds averaged Navier-Stokes equations in general form, using the SIMPLE finite volume method over a non-uniform staggered grid, including the jet channel. Their results of two different turbulence models used (standard k ε with wall function and zonal $(k$ $\varepsilon)/(k$ $\omega)$) were compared with the previous existing computational and experimental results for three different velocity ratios of 0.5, 1.0 and 1.5. They reported that the mean velocity profiles agreed well with the experimental data, whereas there were some discrepancies in the turbulence kinetic energy profiles.

Acharya et al. [7] studied the capabilities of different predictive methods (k ε models, Reynolds Stress Transport Model (RSTM), Large Eddy Simulation (LES) and DNS) in correctly calculating the measured statistics of a film cooling jet in a cross flow. They only simulated the cross flow and applied the experimental inlet boundary condition at the jet exit. They reported that two-equation models usually underpredict the lateral spreading of the film cooling

jet and overpredict its vertical prediction. Their RSTM predictions were not substantially better than their two-equation model predictions. Finally, they reported that the LES and DNS predictions were better able to predict the mean velocities and the turbulent stresses.

Kapadia et al. [8] simulated a streamwise 35° inclined row of round jets, injected on a flat plate for a blowing ratio of 1.0 and a density ratio of 2.0, using the Detached Eddy Simulation (DES) approach. They showed that the DES time averaged solution is able to closely depict the dynamic nature of the flow. Also, they reported that comparison between the experimental and DES time averaged effectiveness was satisfactory. However, numerical values of centerline and span averaged effectiveness differ from those of experimental values at downstream locations.

In the present work, the emphasis is on the effects of the velocity ratio. Note that, in film cooling applications, the jet penetration needs to be minimized, whereas, in pollutant dispersion and gas injection in combustors, it needs to be maximized. Since the focus of this paper is on film cooling applications, low velocity ratios are considered.

GOVERNING EQUATIONS

The dimensionless Navier-Stokes equations for incompressible, three-dimensional and time-dependent flow are, as follows:

$$\partial_i u_i = 0,$$

$$\partial_t u_i + \partial_k (u_i u_k) = \quad \partial_i p + \frac{1}{\mathrm{Re}} \partial_{kk} u_i. \tag{1}$$

The governing LES equations are obtained by filtering the above equations. Filtration is a process by which all scales smaller than a selected size, e.g., grid size, are eliminated from the total flow and, hence, the resolvable part of the flow is defined. This process is accomplished using a general filter function in space to limit the range of scales in the flow field. The one dimensional filter function procedure is:

$$\overline{f}(x) = \frac{1}{\Delta x} \int f(x_1) G(x, x_1) dx_1,$$

$$\overline{f}(x) = f(x) \quad f'(x), \tag{2}$$

where $f'(x)$ is the subgrid scale (SGS) component of the flow variable, $f(x)$. Applying the above filter operation to the Navier-Stokes equations, the LES equations are derived as:

$$\partial_i \overline{u}_i = 0,$$

$$\partial_t \overline{u}_i + \partial_k (\overline{u}_i \overline{u}_k) = \quad \partial_i \overline{p} + \frac{1}{\mathrm{Re}} \partial_{kk} \overline{u}_i \quad \partial_j \tau_{ij}. \tag{3}$$

The effects of the small scales are present throughout the SGS stress tensor,

$$\tau_{ij} = (\overline{u_i u_j} \quad \overline{u}_i \overline{u}_j), \tag{4}$$

which requires to be modeled [15-19].

SUBGRID SCALE MODEL

The key to the success of LES is to accurately model the unresolved SGS stresses. There are a number of SGS models varying in complexity from eddy-viscosity to one-equation models. The most widely used model in the LES approach was suggested by Smagorinsky in 1963 [20,21]. This model, which was later called the Smagorinsky model, is based on Boussinesq's approximation, in which the anisotropic part of the SGS stress tensor is related to the strain rate tensor of the resolved fields through an eddy viscosity coefficient [17,18], i.e.:

$$\tau_{ij} \quad \frac{\delta_{ij}}{3} \tau_{kk} = \quad 2\nu_t \overline{S}_{ij}, \tag{5}$$

where ν_t is the eddy viscosity. This quantity is computed from the resolved strain rate tensor magnitude and a characteristic length scale, as follows:

$$\nu_t = l \left|\overline{S}\right| = (C_S \Delta x)^2 \left|\overline{S}\right|, \tag{6}$$

where l is a characteristic length scale and is assumed to be proportional to the filter width, via a Smagorinsky coefficient, C_s. Since the computational grid is stretched near the solid walls, Δx has to be replaced by an average Δx_{ave} of the individual grid sizes, Δx_i. For meshes with moderate anisotropies, the proper average is the geometric mean, as follows:

$$\Delta x_{\mathrm{ave}} = (\Delta x \Delta y \Delta z)^{1/3}, \tag{7}$$

which usually works well up to aspect ratios of about 20:1 [22]. Note that $\left|\overline{S}\right|$ is the absolute value of the resolved strain rate tensor, i.e.:

$$\left|\overline{S}\right| = (2\overline{S}_{ij} \overline{S}_{ij})^{1/2}, \tag{8}$$

and,

$$\overline{S}_{ij} = \frac{1}{2} \left(\frac{\partial \overline{u}_i}{\partial x_j} + \frac{\partial \overline{u}_j}{\partial x_i} \right). \tag{9}$$

Note that the Smagorinsky coefficient, C_S, varies from 0.1 to 0.25 [23]. Lilly showed that, under idealized conditions, the Smagorinsky model is consistent with an infinitely extended inertial subrange [22]. By conducting analysis only for an infinitely extended inertial subrange and a cut-off filter, Lilly derived that:

$$C_S = \frac{1}{\pi} (\frac{2}{3\alpha})^{3/4}. \tag{10}$$

Refined theoretical studies for more realistic spectra and other filter functions did not reveal a considerable sensitivity of the value of the Smagorinsky constant. Assuming a Kolmogorov constant of $\alpha = 1.5$, one finds $C_S \approx 0.17$. It should be noted that, in the present work, the Smagorinsky constant is assumed as being 0.17. In regions close to a rigid wall, the Van Driest damping function is used to get the correct near wall behavior:

$$C_{S\,\text{wall}} = C_S(1 \quad \exp(\ \ y^+/A^+))^{1/2}, \tag{11}$$

where y^+ is the distance from the wall in viscous wall units and A^+ is a dimensionless constant, usually set to the value of $A^+ = 25$ [21,22].

The basis for the Smagorinsky model is the assumption that the subgrid stress tensor is a scalar product of the strain rate tensor. Therefore, the energy can only be transferred from the resolved scales to the subgrid ones and there would be no backscattering of energy. If the Smagorinsky constant is chosen properly, this model may dissipate the correct ensemble-averaged energy from the resolved scales. However, the model may remove too much or less energy locally, even though the net energy dissipation could be correct. To address some of these drawbacks, the dynamic eddy viscosity and dynamic one-equation models are introduced.

In the dynamic eddy viscosity model, the universal model coefficients are dynamically determined from the resolved field as a function of both time and space. The dynamic coefficients obtained in this manner may be positive or negative. A positive coefficient implies that energy flows from the resolved to the subgrid scales, whereas a negative coefficient implies that energy flows from the subgrid scales to the resolved scales. Whereas this backscattering behavior has a physical basis, in practice, it can be excessive, which can lead to numerical instability [24].

In the dynamic one-equation model, a transport equation for the subgrid turbulent energy is added to the dynamic eddy viscosity model to enforce a budget on the energy flow between the resolved and the subgrid scales, to overcome the numerical instability associated with the dynamic eddy viscosity model. It should be noted that, in order to obtain the dynamic SGS coefficient in this model, one encounters a single Fredholm integral equation of the second type, which can be solved using an iterative method. However, the solvability of this integral formulation is not addressed and there are indications that the iterative solution for the dynamic coefficient does not always converge [24] and requires more effort. Furthermore, the application of dynamic subgrid scale models requires more computer time and memory. Therefore, the Smagorinsky subgrid scale model is used in this work.

COMPUTATIONAL METHODOLOGIES

The simulations are performed using an inhouse computer code, which has been developed by the present authors. Code verification studies are performed using two- and three-dimensional cavity flows. In the two-dimension cavity, the flow is simulated at Reynolds numbers of 1000 and 10000 and the results are compared with the benchmarks of Ghia and Ghia [25], which show excellent agreement [26]. In the three-dimensional case, cavity flow is simulated at Reynolds numbers of 3200 and 10000 and the results are compared with the experimental results of Prasad and Koseff [27], showing good agreement [28].

The proposed computational domain and its boundary conditions and the computational grid are shown in Figures 1 and 2, respectively. The Cartesian coordinate system is used in which X is parallel to the cross flow direction, Y is parallel to the initial jet flow direction and Z is perpendicular to the XY-plane. Note that the origin of the coordinate system is located on the geometrical center of the jet exit. The cross flow boundary layer thickness used was the same as that used in Ajersch's experimental work ($\delta = 2D$), with a 1/7 power law profile and the jet inlet velocity was considered to be uniform. As shown in Figure 1, a single square cross-section jet was considered in the computational domain. To impose the influences of the other jets, the periodic boundary condition was used in the Z-direction.

The computational grid used is non-uniform in

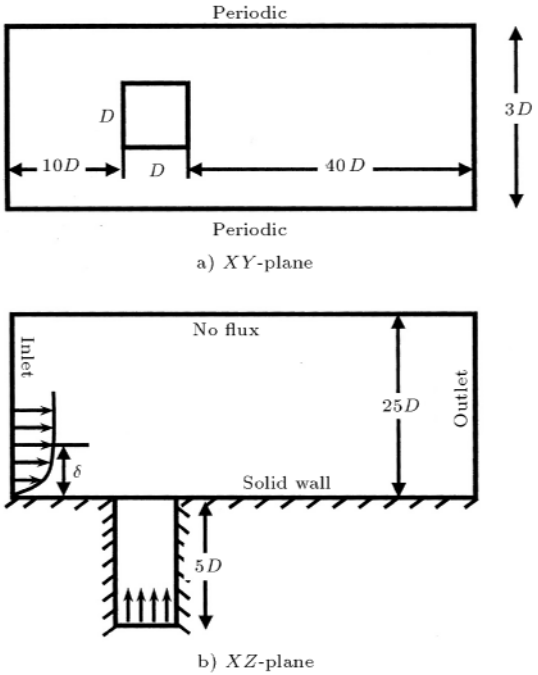

Figure 1. Computational domain and its boundary conditions.

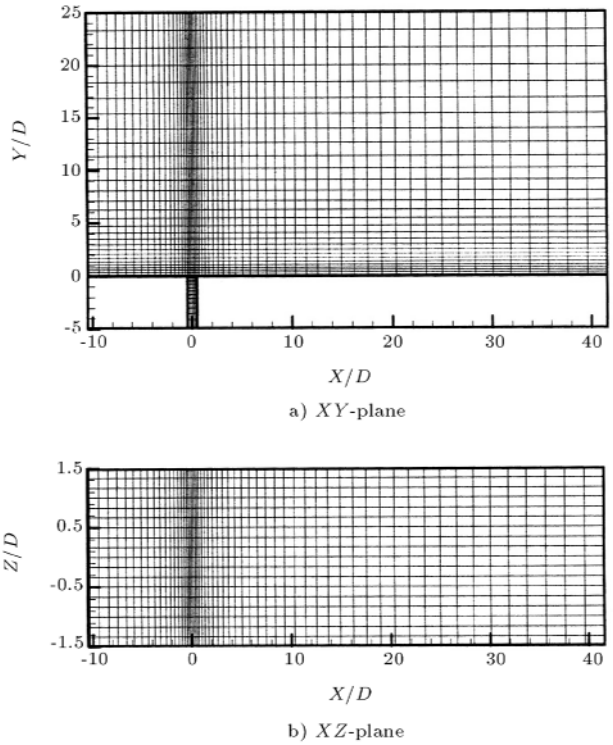

Figure 2. Computational grid.

Y-directions, where the grid points are clustered near the walls, using the following algebraic stretching function [29]:

$$Y = H\frac{(\beta+1) \quad (\beta \quad 1)\{[(\beta+1)/(\beta \quad 1)]^{(1 \quad \eta)}\}}{[(\beta+1)/(\beta \quad 1)]^{(1 \quad \eta)}+1}, \tag{12}$$

where η and β are the metric and the clustering coefficient, respectively. Also, grid refinement is performed in an X-direction in the cross flow block. That is, the grid is stretched close to the jet exit and expanded away from it. In the Z-direction, a uniform grid is used in both blocks. Note that, in the interface of the two blocks, the grid points of the two blocks intersect.

The grid resolution study is performed using different grid arrangements, as given in Table 1. Maximum and minimum grid spacings are shown in Table 2 for the two blocks. The third grid in the above mentioned tables is selected for the simulation. An incompressible finite volume method, using an unsteady SIMPLE algorithm and implying a multiblock staggered grid arrangement, is also used. All spatial terms in the Navier-Stokes equations are discretized using the Power-Law scheme. The Crank-Nicolson scheme is also used for discretization of the temporal terms [30]. Also, the uniform time step of $\Delta t = 0.01$ is considered for time marching up to $t = 70$ seconds. Each iteration takes nearly 13 seconds. Nearly 12,000 iterations are needed for the convergence and 7,000 iterations are needed for time marching. The simulations are performed using a personal computer with a Pentium VI processor and a 512 mega-bytes memory and no parallel processing has been applied. Note that the time averages of the results are used for investigations.

Table 1. Grid arrangements for grid resolution study.

Blocks	Jet Flow Block			Cross Flow Block		
Direction	X	Y	Z	X	Y	Z
First Grid	7	18	5	80	40	13
Second Grid	9	18	7	100	50	19
Third grid	11	23	9	120	60	25
Fourth Grid	13	28	11	140	70	31

RESULTS

In this work, the jet behavior in a cross flow, at three different velocity ratios, namely, 0.5, 1.0 and 1.5, has been computationally simulated using the LES approach. No temperature difference between the jet and the cross flow is considered. The jet Reynolds number is taken to be 4700 and, thus, the injected flow is turbulent. Note that, in almost all previous works [7], the cross flow alone has been solved using an existing boundary condition at the jet exit, while, as explained here, it seems to be necessary to solve the flow in the jet channel along with the cross flow, simultaneously.

In Figures 3 to 5, the results of the mean velocity profiles of $< \overline{U} >$, $< \overline{V} >$ and $< \overline{W} >$ versus Y, for different streamwise locations ($X/D = 0.0$, 1.0, 3.0 and 5.0) at $R = 0.5$, are shown, respectively. These results are compared with the experimental and computational results of Ajersch et al. [3].

In Figure 3, the computed mean streamwise velocity profiles, $< \overline{U} >$, at different X-locations, at $Z/D = 0.0$ are shown for $R = 0.5$. It should be noted that the agreement between obtained and experimental results is excellent in comparison with the computational profiles of Ajersch et al. However, by increasing X, there would be a minor deviation between the present computational data and the experimental work of Ajersch et al., but, even so, the agreements are better than the above mentioned computational results. This may be due to the fact that the grid is stretched near the jet exit. It, therefore, shows that the LES approach has shown its ability to predict the rapid variations near the wall; while the Reynolds Averaged Navier-Stokes (RANS) results of Ajersch et al. have some major difficulties in this respect.

In Figure 4, the computed mean vertical velocity profiles, $< \overline{V} >$, at different X-locations, at $Z/D = 1.0$, are shown for $R = 0.5$. The agreement between present and experimental results is not excellent. That is, in Figure 4a, the obtained results show weak agreement with the experimental ones, in comparison

Table 2. The maximum and minimum grid spacing in each direction for both blocks.

Parameter	Minimum Grid Spacing			Maximum Grid Spacing		
	ΔX	ΔY	ΔZ	ΔX	ΔY	ΔZ
First Grid	0.1667	0.1667	0.1667	2.0700	1.6784	0.1667
Second Grid	0.1250	0.1216	0.1250	1.4931	1.2488	0.1250
Third Grid	0.1000	0.0959	0.1000	1.1911	0.9942	0.1000
Fourth Grid	0.0833	0.0791	0.0833	0.9994	0.8258	0.0833

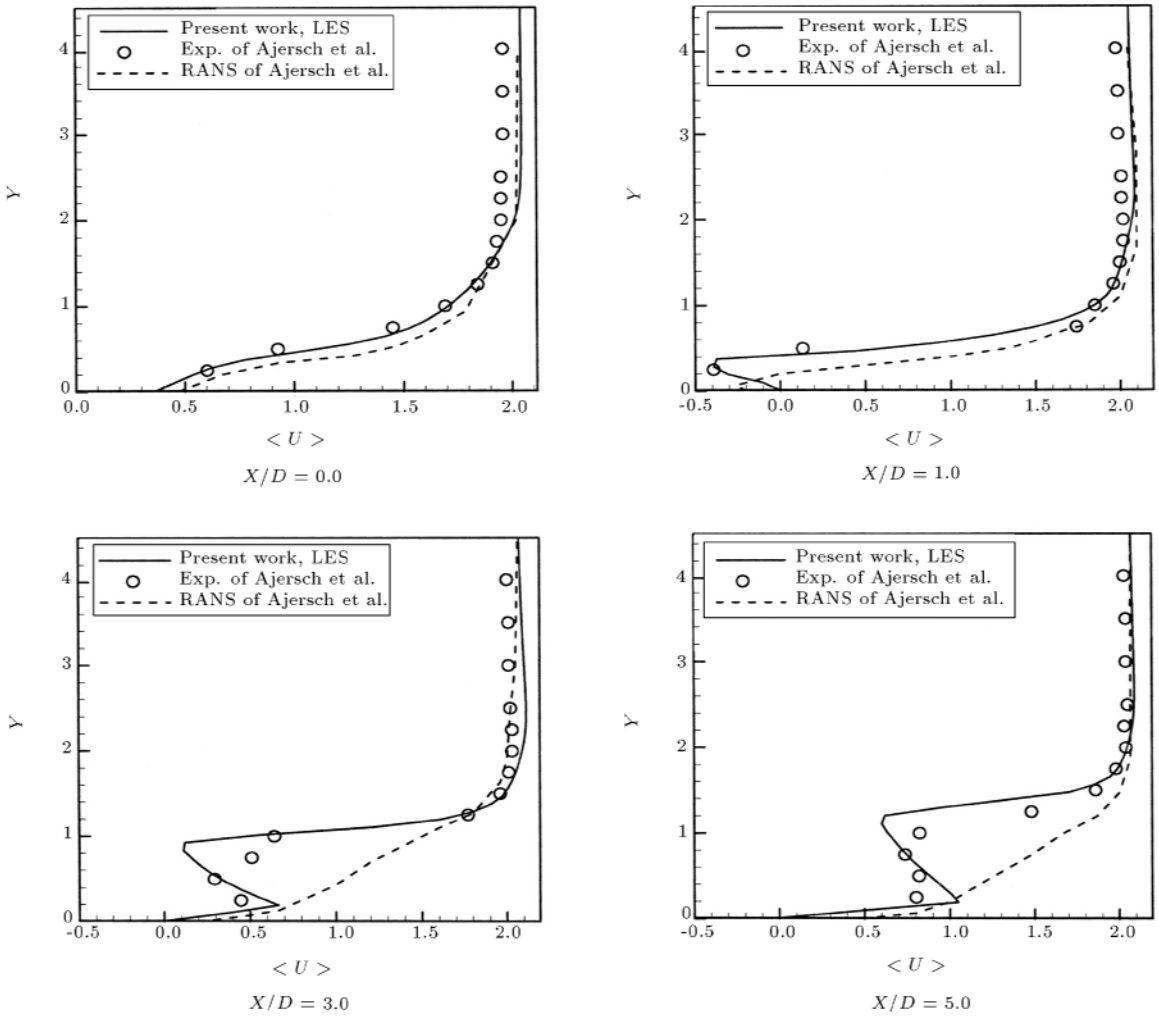

Figure 3. $< \overline{U} >$-velocity profiles of $R = 0.5$ at different YZ-planes ($X/D = 0.0$, 1.0, 3.0 and 5.0) at $Z/D = 0.0$ plane.

with the computational results of Ajersch et al. at $Y < 0.7$. However, better agreement is obtained at higher Y. In Figures 4b to 4d, the results are improved and better agreement is obtained. It is shown that, near the jet exit, the rapid variations near the wall, which seem to be reasonable, are, again, predicted by the LES approach. Of course, here, there are not enough existing experimental data with which to compare the authors' results.

In Figure 5, the computed mean spanwise velocity profiles, $< \overline{W} >$, at different X-locations, at $Z/D =$ 0.5, are shown for $R = 0.5$. It is also noted that the agreement between the present profiles and the experimental data is relatively good. In Figure 5a, the obtained results show weak agreement with the experimental ones, in comparison with the computational results of Ajersch et al. However, in Figures 5b to 5d, the results are improved and better agreement is obtained at $Y < 0.7$. As shown, at the jet exit, the peak of the variations predicted by the authors LES

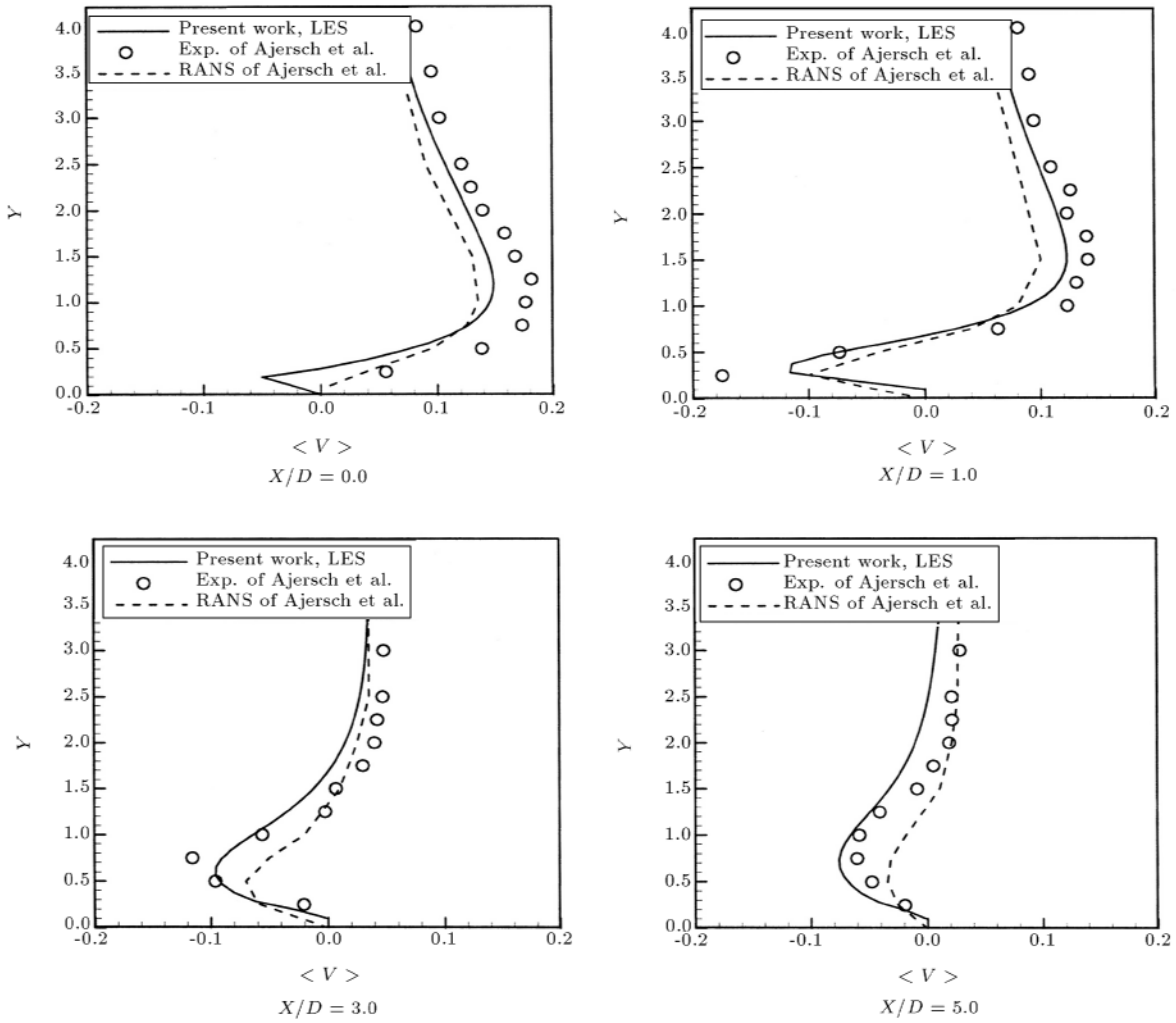

Figure 4. $< \overline{V} >$-velocity profiles of $R = 0.5$ at different YZ-planes ($X/D = 0.0$, 1.0, 3.0 and 5.0) at $Z/D =$ 1.0 plane.

results is approximately -0.72, while this value is -0.76 from the RANS results of Ajersch et al. Although there are no experimental data with which to compare, from other comparisons, the LES value seems to be closer to the corresponding experimental results.

Generally speaking, the present LES results are extremely close to the existing experimental results. However, in some cases, the RANS simulations show some improvement over the LES. It should be noted that, in the k ε model of the RANS simulation, there are several flow dependent constants that are adjusted and which play the role of improving the results. In the LES, only the Smagorinsky constant could be adjusted, the value of which is obtained from Equation 10. Therefore, the existing small discrepancies may be due to the deficiencies of the Smagorinsky SGS model. This model is based on the eddy viscosity assumption and only dissipates the energy, not allowing the backscattering of the energy from the small scales to the large scales. That is to say, it is more dissipative near the solid walls, but, as can be seen from the above figures, here, this error can be ignored. Of course, using dynamic subgrid scale models, which require more computer time and memory, can improve the accuracy significantly.

In Figures 6 to 8, the time-mean velocity vectors in three different YZ-planes of X/D = 1.0, 3.0 and 5.0, for three respective velocity ratios of $R = 0.5$, 1.0 and 1.5, are shown. As the velocity ratio increases, the jet to cross flow momentum ratio increases. This causes the jet to penetrate more into the cross flow. On the other hand, for all three velocity ratios, as the distance at an X-direction from the jet exit increases, the jet flow detaches more from the wall. Therefore, as expected, at further distances from the jet exit, the Counter Rotating Vortex Pairs (CRVP) get further away from the wall. At the same time, the distance between the CRVP centers in the spanwise direction varies.

Figure 6 shows that, as the distance at an X-

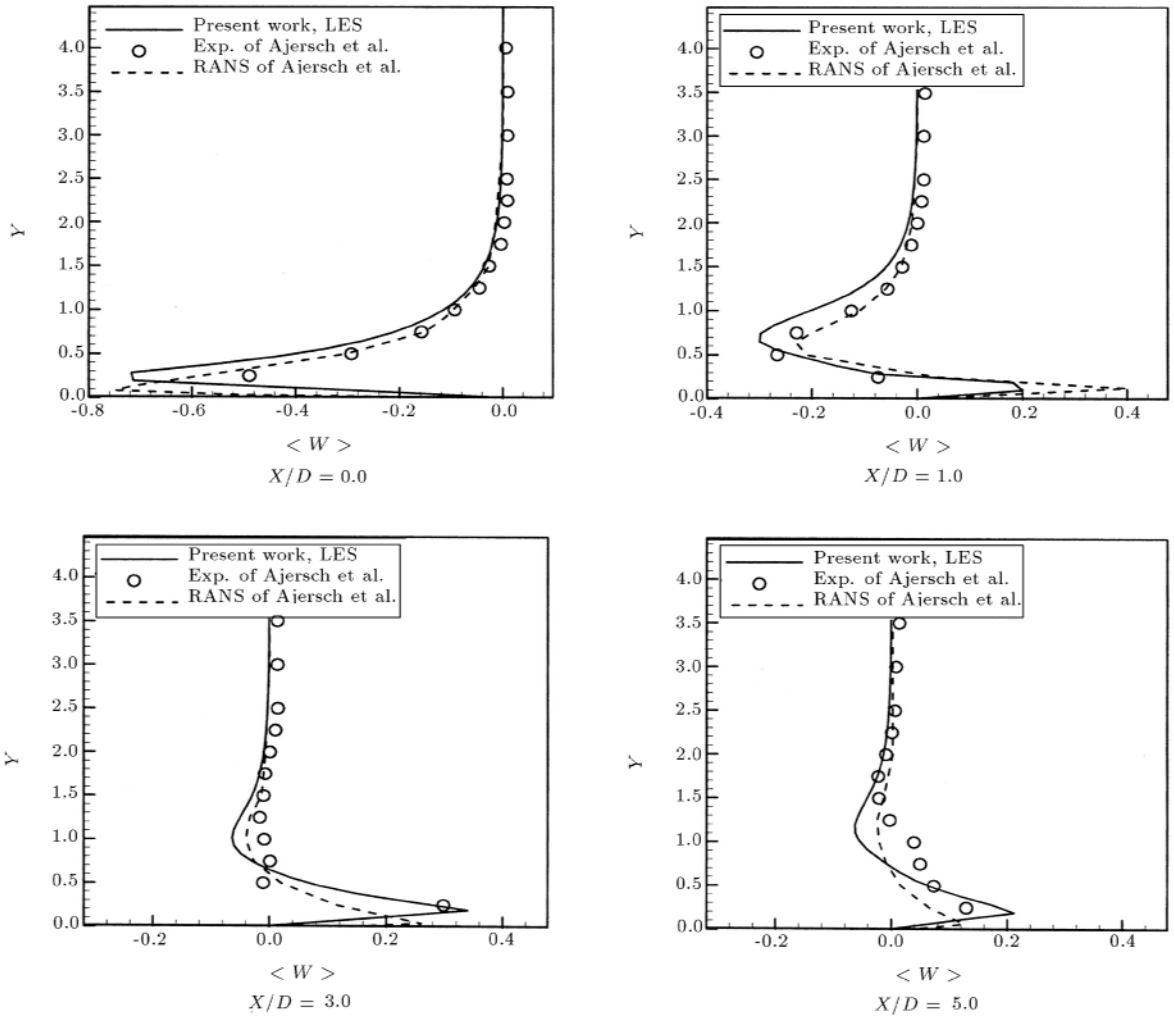

Figure 5. $< \overline{W} >$-velocity profiles of $R = 0.5$ at different YZ-planes ($X/D = 0.0$, 1.0, 3.0 and 5.0) at $Z/D =$ 0.5 plane.

direction from the jet exit increases, the centers of the CRVP get further away from the wall. That is, the CRVP centers in the Y-direction are located at 0.22, 0.49 and 0.65, at $X/D = 1.0$, 3.0 and 5.0, respectively. This flow feature could be observed at the higher velocity ratios of Figures 7 and 8. Therefore, the centers are located at $Y/D = 0.43$, 0.92 and 1.14, for $R = 1.0$ and at $Y/D = 0.5$, 1.03 and 1.38, for $R = 1.5$ at the corresponding $X/D = 1.0$, 3.0 and 5.0, respectively. It is concluded that, as the distance from the jet exit increases, the Y-position of the CRVP centers increases at all velocity ratios.

The spanwise distance between the CRVP centers decreases as the distance from the jet exit increases at $R = 0.5$. These distances are 1.3, 0.73 and 0.71 at $X/D = 1.0$, 3.0 and 5.0, respectively. However, at $R = 1.0$ and 1.5, this flow feature is observed, except for $X/D = 5.0$. At $R = 1.0$, the spanwise distances between the centers are 1.36, 0.73 and 1.0 and at $R = 1.5$, these distances are 1.65, 0.92 and 0.98 at the corresponding $X/D = 1.0$, 3.0 and 5.0, respectively. This behavior is due to the fact that, at higher velocity ratios, the CRVP expands more and touches the spanwise periodic boundary at a lower X after the jet exit.

When the velocity ratio is low, the jet flow is bent towards the wall at each side. Thus, only the jet flow will be in contact with the wall. Furthermore, near the jet exit, the jet penetration is negligible and so is its mixing with the cross flow fluid. It can be concluded that, in film cooling applications, the velocity ratio must be low. Of course, there are other parameters, like injection angle and injection geometry etc., which must be optimized. At higher velocity ratios, the cross flow fluid comes under the jet flow from each side and pushes it up; therefore, its penetration is considerable. So, in this situation, the jet to cross flow mixing is high and the cross flow will be in contact with the surface.

After the jet enters the cross flow, it becomes very vortical. Actually, highly strong vortical regions, i.e.

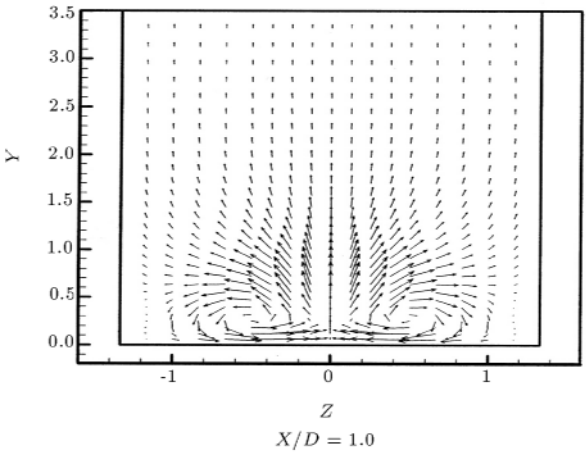

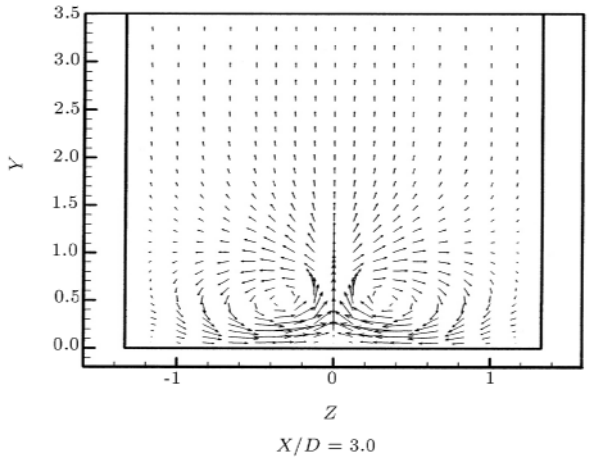

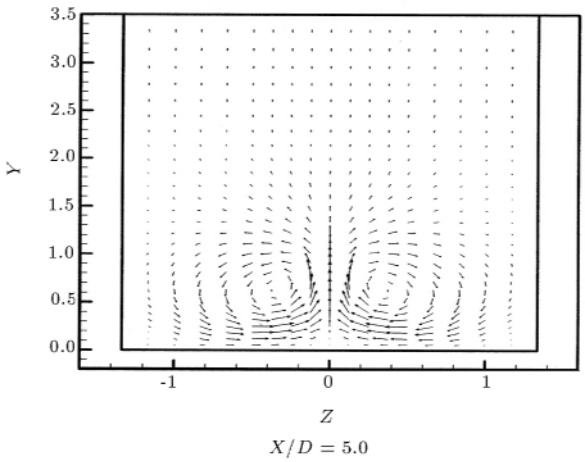

Figure 6. Time-mean velocity vectors in different YZ-planes ($X/D = 1.0$, 3.0 and 5.0) at $R = 0.5$.

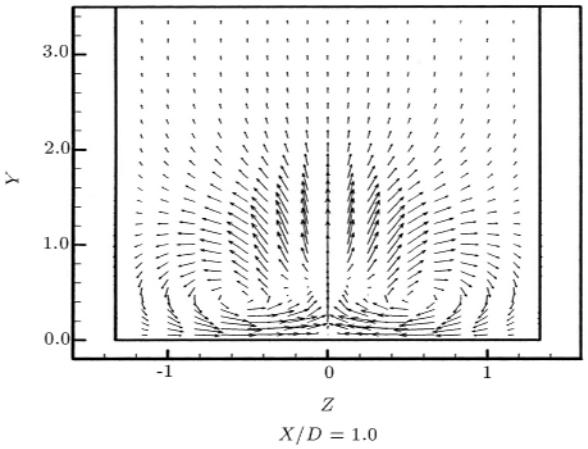

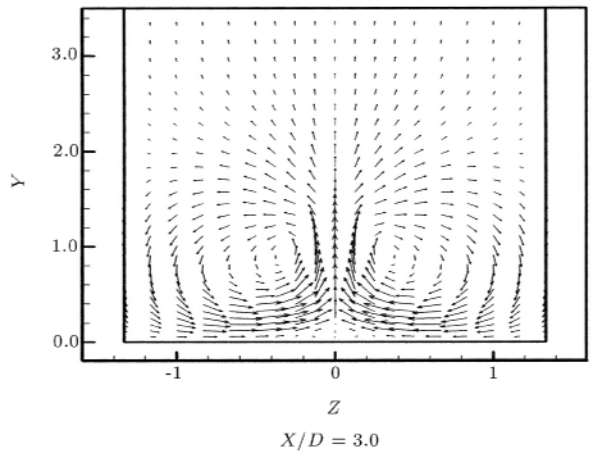

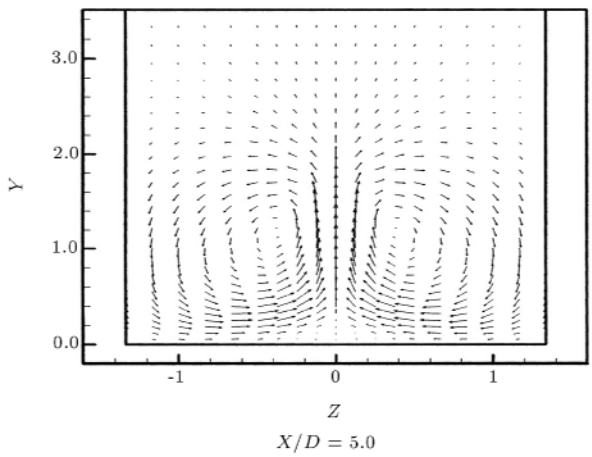

Figure 7. Time-mean velocity vectors in different YZ-planes ($X/D = 1.0$, 3.0 and 5.0) at $R = 1.0$.

the CRVP, will be formed, which will be dissipated far from the jet exit. The main influence of this vortical motion is to mix the jet with the cross flow. So, in film cooling applications, it is desirable to decrease such vortical motion by optimizing the velocity ratio and the other effective parameters. On the other hand, in problems such as pollutant dispersion, gas injection in combustors and the mixing of liquids/gases, the objective is to generate these vortical regions as soon and as strong as possible.

CONCLUSIONS

The jet penetration and mixing characteristics of mul-

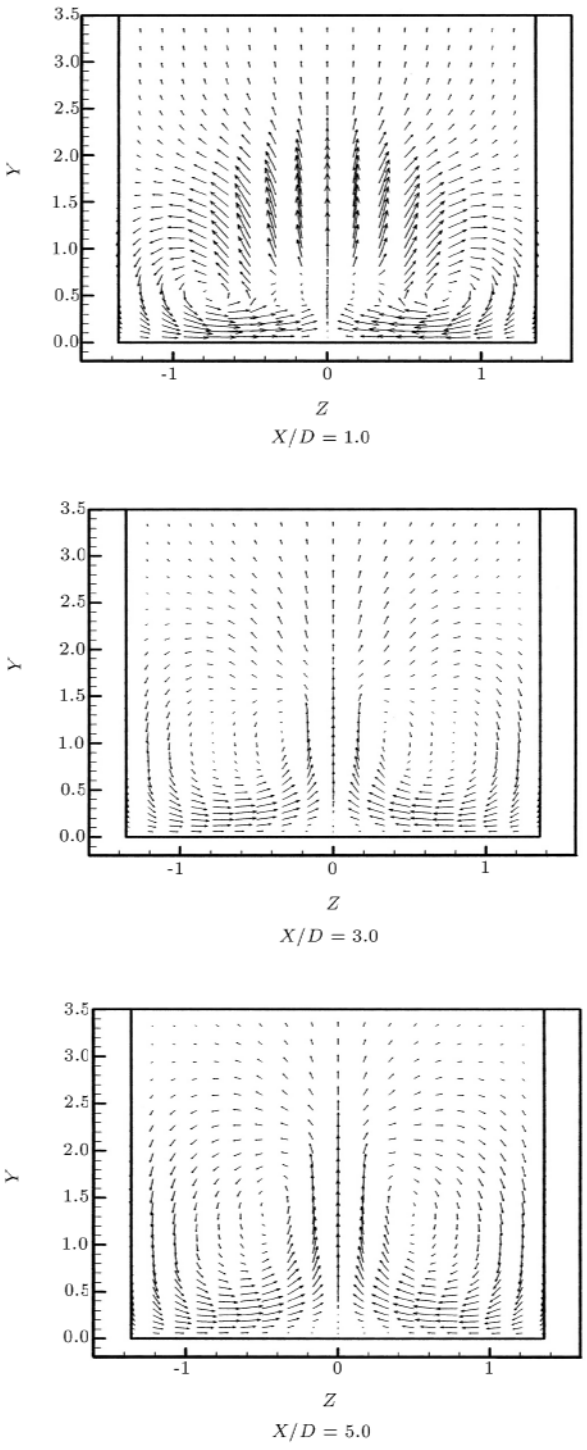

Figure 8. Time-mean velocity vectors in different YZ-planes ($X/D = 1.0$, 3.0 and 5.0) at $R = 1.5$.

tiple square cross section jets into a cross flow on a flat plate, at three different velocity ratios of 0.5, 1.0 and 1.5, are studied, using the LES approach. The LES results are in much better agreement with the existing experimental results, in comparison with the relevant computational results of the RANS approach. After the jet enters the cross flow, it generates counter rotating vortex pairs, expands and penetrates to the cross flow in the YZ-plane. The results show that:

1. By increasing the velocity ratio, the jet penetration into the cross flow is increased, accompanied by high mixing with the cross flow;
2. After the jet enters the cross flow, it forms highly vortical regions, which are called Counter Rotating Vortex Pairs (CRVP);
3. As the distance in an X-direction from the jet exit increases, the Y-position of the CRVP centers increases at all velocity ratios;
4. The spanwise distance between the CRVP centers decreases before the CRVP touches the spanwise periodic boundary;
5. The main influence of these vortical behaviors is to mix the jet with the cross flow;
6. The CRVP gets stronger, as the velocity ratio increases. Therefore, it is suggested that, in film cooling applications, low velocity ratio and, inversely, in flows such as pollutant dispersion, gas injection in combustors and the mixing of liquids/gases applications, high velocity ratios, are to be applied.

REFERENCES

1. Andreopoulos, J. "On the structure of jets in a cross-flow", *Journal of Fluid Mechanics*, **157**, pp 163-197 (1985).
2. Lee, S.W., Lee, J.S. and Ro, S.T. "Experimental study on the flow characteristics of streamwise inclined jets in crossflow on flat plate", *Journal of Turbomachinery*, **116**, pp 97-105 (1994).
3. Ajersch, P., Zhou, J.M., Ketler, S., Salcudean, M. and Gartshore, I.S. "Multiple jets in a crossflow: Detailed measurements and numerical simulations", *International Gas Turbine and Aeroengine Congress and Exposition*, ASME Paper 95-GT-9, Houston, Texas, USA, pp 1-16 (1995).
4. Holdman, J.D. and Walker, R.E. "Mixing of a row of jets with a confined crossflow", *AIAA Journal*, **15**(2), pp 243-249 (1977).
5. Hoda, A. and Acharya, S. "Predictions of a film coolant jet in crossflow with different turbulence models", *Journal of Turbomachinery*, **122**, pp 558-569 (2000).
6. Keimasi, M.R. and Taeibi-Rahni, M. "Numerical simulation of jets in a crossflow using different turbulence models", *AIAA Journal*, **39**(12), pp 2268-2277 (2001).
7. Acharya, S., Tyagi, M. and Hoda, A. "Flow and heat transfer predictions for film cooling", *Heat Transfer in Gas Turbine Systems, Annals of the New York Academy of Sciences*, **934**, pp 110-125 (2001).

8. Kapadia, S., Roy, S. and Heidmann, J. "Detached eddy simulation of turbine blade cooling", *36th Thermophysics Conference*, AIAA-2003-3632, Orlando, Florida, USA, pp 1-10 (2003).
9. Hass, W., Rodi, W. and Schonung, B. "The influence of density difference between hot and coolant gas on film cooling by a row of holes: Predictions and experiments", *Journal of Turbomachinery*, **114**, pp 747-755 (1992).
10. Honami, S., Shizawa, T. and Uchiyama, A. "Behavior of the laterally injected jet in film cooling: Measurements of surface temperature and velocity/temperature filed within the jet", *Journal of Turbomachinery*, **116**, pp 106-112 (1994).
11. Hassan, I., Findlay, M., Salcudean, M. and Gartshore, I. "Prediction of film cooling with compound-angle injection using different turbulence models", *6th Annual Conference of the Computational Fluid Dynamics Society of Canada*, Quebec, Canada, pp 1-6 (1998).
12. Amer, A.A., Jubran, B.A. and Hamdan, M.A. "Comparison of different two-equation turbulent models for prediction of film cooling from two rows of holes", *Numerical Heat Transfer*, Part A, **21**, pp 143-162 (1992).
13. Thole, K., Gritsch, M., Schulz, A. and Witting, S. "Flowfield measurements for film-cooling holes with expanded exits", *Journal of Turbomachinery*, **120**, pp 327-336 (1998).
14. Schmidt, D.L. and Bogard, D.G. "Pressure gradient effects on film cooling", *International Gas Turbine and Aeroengine Congress and Exposition*, ASME Paper 95-GT-18, Houston, Texas, USA, pp 1-8 (1995).
15. Ramezanizadeh, M. and Taeibi-Rahni, M. "Large eddy simulation of three-dimensional cavity flow using Smagorinsky model", *First International and Third Biennial Conference of the Iranian Aerospace Society*, Sharif University of Technology, Tehran, Iran, **4**, pp 99-106 (2000).
16. Ghosal, S. "Mathematical and physical constraints on LES", *AIAA*, Paper 98-2803, pp 1-13 (1998).
17. Ramezanizadeh, M. and Taeibi-Rahni, M. "Large eddy simulation of a two-dimensional flat plate film-cooling", *The Ninth Asian Congress of Fluid Mechanics*, Isfahan University of Technology, Isfahan, Iran, pp 1-7 (2002).
18. Tafti, D.K., Zhang, X., Huang, W. and Wang, G. "Large-eddy simulations of flow and heat transfer in complex three-dimensional multilouvered fins", *ASME Fluids Engineering Division Summer Meeting*, FEDSM2000-11325, Boston, Massachusetts, USA, pp 1-18 (2000).
19. Sohankar, A. and Davidson, L. "Large eddy simulation of turbulent flow over a square prism by using two subgrid-scale models", *4th International and 8th Annual Conference of Iranian Society of Mechanical Engineers*, Sharif University of Technology, Tehran, Iran, **3**, pp 551-558 (2000).
20. Iliescu, T. and Fischer, P. "Backscatter in the rational LES model", *J. Computers and Fluids*, **33**, pp 783-790 (2004).
21. Meinke, M., Schroder, W., Krause, E. and Rister, T. "A comparison of second- and sixth-order methods for large-eddy simulations", *J. Computers and Fluids*, **31**, pp 695-718 (2002).
22. Peyret, R., *Handbook of Computational Fluid Mechanics*, San Diego, Academics Press (1996).
23. Zhang, W. and Chen, Q. "Large eddy simulation of indoor airflow with a filtered dynamic subgrid scale model", *International Journal of Heat and Mass Transfer*, **43**, pp 3219-3231 (2000).
24. Pomraning, E. and Rutland, C. "Dynamic one-equation nonviscosity large-eddy simulation model", *AIAA Journal*, **40**(4), pp 689-701 (2002).
25. Ghia, U., Ghia, K.N. and Shin, C.T. "High-Re solutions for incompressible flow, using the Navier-Stokes equations and a multigrid method", *J. Comp. Phys.*, **387**, pp 387-411 (1982).
26. Ramezanizadeh, M., *Large Eddy Simulation of Film Cooling in a Turbulent Flow Over a Flat Plate*, MSc. Thesis, Aerospace Eng. Dept., Sharif University of Technology, Tehran, I.R. Iran (2000).
27. Zang, Y., Street, R.L. and Koseff, J.R. "A dynamic mixed subgrid-scale model and its application to turbulent recirculating flows", *Phys. Fluids A*, **5**(12), pp 3186-3096 (1993).
28. Taeibi-Rahni, M. and Ramezanizadeh, M. "Investigation of three-dimensional cavity flow using large eddy simulation", *J. Aerospace Science and Technology*, **2**(2), pp 1-10 (2005).
29. Hoffmann, K.A. and Chiang, S.T. "Computational fluid dynamics for engineers", *Engineering Education Science*, **1**, USA, Chapter 9, pp 470-471 (2000).
30. Versteeg, H.K. and Malalasekara, W., *An Introduction to Computational Fluid Dynamics-The Finite Volume Method*, Longman Malaysia, Chapters 5-7, pp 103-167 (1995).